JACS
JOURNAL OF THE AMERICAN CHEMICAL SOCIETY
Article
pubs.acs.org/JACS

Electric Field Induced Reversible Phase Transition in Li Doped Phosphorene: Shape Memory Effect and Superelasticity

Junkai Deng,*[,†] Zhenyue Chang,[‡] Tong Zhao,[†] Xiangdong Ding,[†] Jun Sun,[†] and Jefferson Zhe Liu*[,‡]

[†]State Key Laboratory for Mechanical Behavior of Materials, Xi'an Jiaotong University, Xi'an, 710049, China
[‡]Department of Mechanical and Aerospace Engineering, Monash University, Clayton, VIC 3800, Australia

Supporting Information

ABSTRACT: Phosphorene, the single-layer form of black phosphorus, as a new member of atomically thin material family, has unique puckered atomistic structure and remarkable physical and chemical properties. In this paper, we report a discovery of an unexpected electromechanical energy conversion phenomenon—shape memory effect—in Li doped phosphorene P_4Li_2, using *ab initio* density functional theory simulations. Two stable phases are found for the two-dimensional (2D) P_4Li_2 crystal. Applying an external electric field can turn on or off the unique adatom switches in P_4Li_2 crystals, leading to a reversible structural phase transition and thereby the shape memory effect with an tunable strain output as high as 2.06%. Our results demonstrate that multiple temporary shapes are attainable in one piece of P_4Li_2 material, offering programmability that is particularly useful for device designs. Additionally, the P_4Li_2 displays superelasticity that can generate a pseudoelastic tensile strain up to 6.2%. The atomic thickness, superior flexibility, excellent electromechanical strain output, the special shape memory phenomenon, and the programmability feature endow P_4Li_2 with great application potential in high-efficient energy conversion at nanoscale and flexible nanoelectromechanical systems.

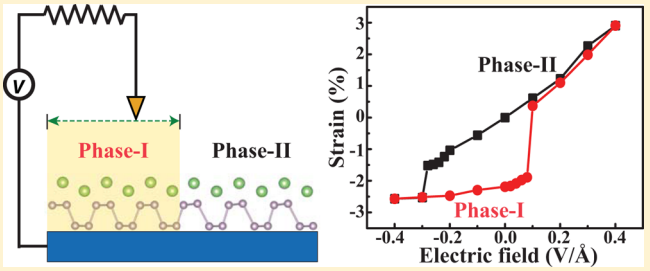

INTRODUCTION

Since the discovery of graphene,[1] two-dimensional (2D) crystals have emerged as a class of materials with unique atomically thin crystal structures and exceptional physical properties, such as extremely lightweight, ultrahigh mechanical strength, excellent flexibility, and anomalous optical and electronic properties.[2−6] Utilization of these 2D materials is leading to remarkably innovative devices for electronics, photonics, and energy applications.[7−11] Particularly, the intrinsic nanosized thickness and superior flexibility render 2D materials indispensable candidates for flexible nano-electromechanical system (NEMS) devices, integrating the electrical and mechanical functionality at the nanoscale for applications such as energy conversion, soft robotics, and bioengineering.[12−18]

In most NEMS devices, electromechanical actuators are the key components, which converts electric energy to mechanical motion. To achieve a large electromechanical actuation strain in 2D materials, three mechanisms have been explored, i.e., piezoelectricity, electroactive effect, and quantum mechanical effect.[18−24] Several promising 2D piezoelectrics, such as single-layer *h*-BN and dichalcogenides (MoX_2 and WX_2 where X = S, Se, Te), have been reported with piezoelectric coefficients of d_{11} = 1—10 pm/V,[20] which is comparable with some high performance bulk piezoelectric ceramics, such as α-quartz (d_{11} = 2.3 pm/V),[25] GaN (d_{33} = 3.1 pm/V),[26] and AlN (d_{33} = 5.1 pm/V).[26] Immersing electrically charged 2D materials (e.g., graphene) in electrolyte will form the electric double layers at their surfaces, resulting in electroactive deformation caused by Coulomb interaction.[18,21−23] The quantum mechanical effect refers to the change of chemical bond length when 2D materials are subject to an electron or hole injection.[16,18,24] Unfortunately, the reported strain outputs of 2D materials from these three mechanisms are mostly limited to the order of 0.1−1.0%.[18,20−24]

Phosphorene, the single-layer form of black phosphorus, is rediscovered as a new member of an atomically thin 2D crystalline material family.[27,28] Its unique puckered structure and remarkable physical and chemical properties have stimulated intensive studies.[27−31] In this paper, we report a discovery of an unexpected electric field triggered shape memory effect (SME) in Li doped phosphorene P_4Li_2, using *ab initio* density functional theory (DFT) simulations. The SME refers to the ability of a material to recover its original shape after being severely deformed into some temporary shapes (usually caused by external stress), when being subjected to appropriate external stimuli (e.g., temperature, stress, etc.). The SME is a well-known phenomenon and a widely used actuation mechanism for many three-dimensional bulk materials,[32] but it has not been reported for 2D materials yet. The observed SME in 2D P_4Li_2 can generate a maximum recoverable strain up to 2.06%. More importantly our results

Received: December 19, 2015
Published: April 4, 2016

DOI: 10.1021/jacs.5b13274
J. Am. Chem. Soc. 2016, 138, 4772−4778

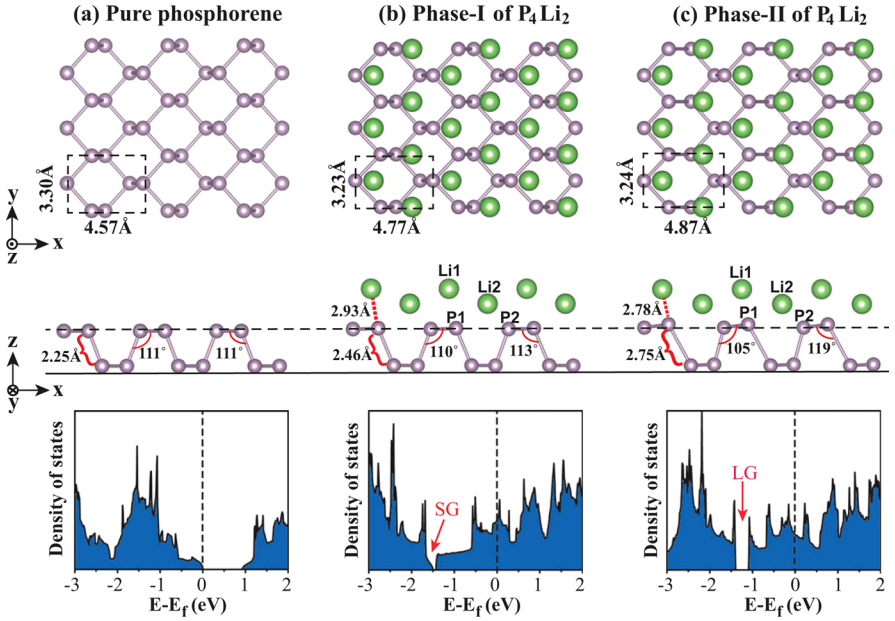

Figure 1. Crystal structures of (a) pristine phosphorene monolayer as well as (b) phase I and (c) phase II of Li doped phosphorene P_4Li_2. The bonding lengths and projected boding angles are labeled to show the key structural difference between the two phases. The electronic density of state results are also shown. Clear differences can be seen at −1.5 eV below the Fermi level: phase I possesses a smaller gap (SG) whereas phase II has a larger gap (LG).

demonstrate the programmability of the P_4Li_2 crystal that is not attainable from other physical mechanisms.

COMPUTATIONAL METHODS

The *ab initio* DFT calculations were performed by use of the Vienna ab initio simulation package (VASP), making use of the generalized gradient approximation (GGA) as implemented by Perdew, Burke, and Ernzerhof (PBE) and the projector augmented wave (PAW) approach.[33,34] The $3s^23p^3$ and $1s^12s^12p^1$ states were treated as valence electrons for P and Li atoms, respectively. The cutoff energy was set as 800 eV. The Monkhorst−Pack special *k*-point method was used with a grid of 25 × 17 × 1 for the rectangular unit cell of phosphorene (Figure 1). A similar *k*-point mesh density was applied to other supercells. Periodic boundary conditions were employed in all DFT calculations. A vacuum layer of 20 Å thickness was used in the *z* direction to minimize interactions between the Li doped phosphorene with its periodic images. The VASP source code was modified to allow the supercells to relax/change in the in-plane directions, meanwhile holding the *z* direction. An electric field was applied perpendicular to the basal plane of phosphorene. All atoms were fully relaxed until the Helmann−Feynman forces were less than 0.001 eV/Å. The HSE06 hybrid functional[35] calculations were also carried out for some cases to confirm the PBE results.

RESULTS AND DISCUSSION

Bistable Phases of Li Doped Phosphorene P_4Li_2. Figure 1a depicts the crystal structure of phosphorene, in which the dashed box represents the unit cell. The phosphorene has a special puckered structure. The calculated in-plane lattice constants are 4.57 Å along the armchair (*x*) direction and 3.30 Å along the zigzag (*y*) direction, respectively. The unit cell includes four P atoms distributed in two atomic layers connected by two types of P−P bonds, a shorter length of 2.22 Å within the same plane and a longer length of 2.25 Å connecting the two atomic planes. The two projected bonding angles are both 111° according to the structural symmetry. The calculated electronic density of state (DOS) clearly shows the semiconducting nature of the monolayer phosphorene with a band gap value of 0.92 eV. Our results for pristine phosphorene are in an excellent agreement with previous work,[27] although the band gap is smaller than the experimental value owing to the well-known fact that DFT calculations often underestimate the band gap results.[36] In our HSE06 calculations, the band gap of pristine phosphorene was corrected to 1.58 eV (Figure S1), which is in reasonable agreement with the reported value.[27]

The hollow site of the hexagonal cell (ring) has been identified as the most stable adsorption site for an alkali adatom on phosphorene.[37] There are two hollow sites on one side of the phosphorene unit cell, i.e., the (0.0, 0.0) and (0.5, 0.5) sites in the projected (001) plane (Figure 1a). We doped two Li adatoms at these two hollow sites on only one side of the phosphorene unit cell. It is interesting that our DFT calculations identify two stable phases for the P_4Li_2 as shown in Figure 1b and 1c, namely phase I and phase II. Their total energy values, −25.267 and −25.276 eV per unit cell, indicate that phase I is a metastable phase.[38] Larger supercells (2 × 2, 3 × 3, and 4 × 4 of P_4Li_2 unit cells) were also examined. The results are consistent with those of the unit cell. Both phase I and phase II are stable. Table S2 lists the lattice constants and total energy results of these supercells. Figure S2 shows the stable structures of the 4 × 4 supercells of both phase I and phase II. Moreover, the Li adsorption energies in the two stable phases are determined to be −1.61 and −1.62 eV per Li atom (Supporting Information), respectively. Both adsorption energy values are lower than the calculated cohesive energy −1.60 eV per Li atom of bulk lithium. Thus, these two phases should be thermodynamically stable against the phase separation into the pure phosphorene and bulk lithium.

In comparison with the pristine phosphorene, the lattice constants of the P_4Li_2 unit cells are expanded to 4.77 and 4.87 Å along the *x* direction and contracted to 3.23 and 3.24 Å along the *y* direction, for phase I and phase II, respectively.[38] Figure 1 and Figure S3 demonstrate detailed structural differences. The upper phosphorene layer in phase I remains planar, whereas

DOI: 10.1021/jacs.5b13274
J. Am. Chem. Soc. 2016, 138, 4772−4778

that of phase II exhibits a clear tilting. Such a tilting is also evidenced by a shorter bond length between the Li1 and P1 atoms in phase II (2.78 Å) than that in phase I (2.93 Å).

Figure 1 also shows the DOS results of both phases. Doping two Li atoms in one unit cell transforms the semiconducting phosphorene (Figure 1a) to a metallic state (Figure 1b and 1c). The most significant DOS difference between the two phases is around −1.5 eV below the Fermi levels. Phase II has a larger band gap (0.4 eV) and sharp band edges, whereas phase I has a smaller band gap (0.1 eV) and profound band tail states. Similar observations were obtained in HSE06 calculations (Figure S1). The intrinsic difference of DOS can be used as a signature to distinguish these two phases.

To gain deeper insights of these two stable phases, we carried out projection DOS calculations (Figure S3), difference-electron density calculations (Figure S3), and Bader analysis (Table S3). In phase II, the two Li adatoms and P1 and P2 atoms show strongly overlapped *s*- and *p*-orbital peaks at both edges of the larger band gap (Figure S3), which is consistent with the stronger charge transfer among these atoms (Table S3). Together with the shorter Li−P interatomic distances (Figure 1 and S3), we can conclude that Li−P interaction is enhanced to form stronger bonding in phase II. The crystal structure also provides some valuable clues. Phase I has a relatively small lattice constant. It appears there is insufficient space to accommodate two Li ions in one unit cell. The Li1 could be repelled by Li2 and move away from phosphorene (Figure 1b). On the other hand, the longer lattice constant of phase II provides more space for Li1, which allows it to get closer to P atoms and form stronger bonding to stabilize phase II.

Electric Field Induced Reversible Phase Transition. Recently there has been growing interest to study the structural phase transition of phosphorene and other 2D materials.[39−41] Barraza-Lopez et al. investigated the phase transitions among 4-fold degenerated ground states (i.e., different crystal orientation) in ridged orthorhombic two-dimensional atomic crystals such as pristine phosphorene and monochalcogenide monolayers.[39] They found that, upon heating the systems up to a transition temperature (T_c), an order-to-disorder phase transition could happen. The disordered phase is a mixture of different ground states. They concluded that the structural order of a free-standing black phosphorene is stable for T_c < 5000 K. Here, for P_4Li_2 crystals, our DFT simulations discover that applying an external electric field (E) perpendicular to the phosphorene basal plane leads to unexpected but interesting structural phase transition between phase I and phase II.

Figure 2 depicts the changes of lattice constants along the armchair (x) and the zigzag (y) directions, with varying electric field strength. The magnitude of the applied electric fields was selected between −0.4 V/Å to 0.4 V/Å that is experimentally achievable in devices made by 2D materials.[7] Phase II exhibits a nearly linear change of lattice constants with respect to electric field strength between −0.3 and 0.4 V/Å. A similar linear relation is observed for phase I between electric field strengths of −0.4 and 0.1 V/Å. This can be attributed to the piezoelectric effect. Fitting the linear relations yields the piezoelectric coefficient d_{31} = 1.1 pm/V for phase I and 6.1 pm/V for phase II. These values are significantly larger than that of other 2D piezoelectric materials such as chemically modified graphene (d_{31} = 0.0018 − 0.3 pm/V)[19] and graphene oxide (d_{31} = 0.24 pm/V)[42] as well as some three-dimensional bulk materials such as wurtzite BN (d_{31} = 0.33 pm/V)[43] and wurtzite

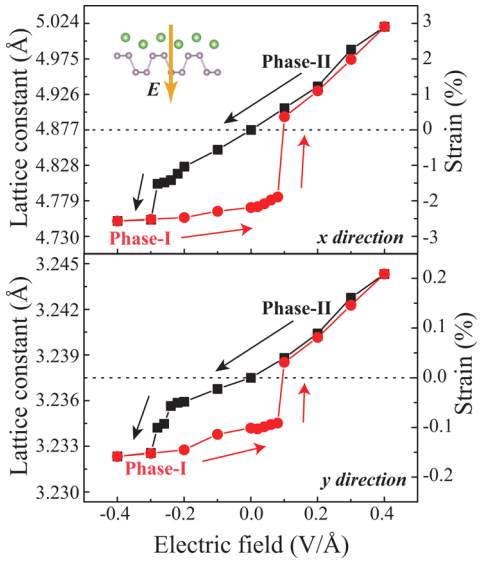

Figure 2. Lattice constant changes along armchair (x) and zigzag (y) directions of P_4Li_2 with varying external electric field that is applied perpendicular to the basal plane. The hysteresis loop of lattice constants represents a reversible electric field induced structural phase transition between two phases. The strain values are calculated as a relative lattice constant change with reference to phase II under a zero electric field.

GaN (d_{31} = 0.96 pm/V),[44] suggesting P_4Li_2 an excellent 2D piezoelectric material.

Interestingly, under an electric field $E \leq -0.3$ V/Å, the lattice constants of phase II suddenly drop to coincide with those of phase I, implying that a phase transition takes place. Indeed, careful DOS analysis shows that under an electric field $E \leq -0.3$ V/Å the relaxed structures display a similar DOS to that of phase I (Figure S4). Note that, upon releasing the electric field, thereafter, the P_4Li_2 crystal remains in phase I instead of recovering to a phase II structure. On the other hand, for phase I, under an electric field $E \geq 0.1$ V/Å, its lattice constants exhibit an abrupt increase to coincide with those of phase II. A careful examination of the DOS results (Figure S4) confirms the phase transition from phase I to phase II. Upon a subsequent release of electric field, the crystal remains in the phase II state instead of recovering to phase I. Figure 2 demonstrates a hysteresis loop of lattice constants upon an external electric field, manifesting an electric field induced reversible structural phase transition.

To gain a better understanding of the observed electric field induced phase transition, Figure 3 shows the relative total energy as a function of x lattice constant under an electric field strength of −0.3, −0.1, 0.0, and 0.1 V/Å, respectively. A characteristic double well energy profile is observed in the case of zero electric field (Figure 3c), where two local minimum points correspond to phase I and phase II (Figure S6), respectively. Applied electric fields change the double well energy profile, altering the relative energetic order of the two phases. Under a relatively low electric field strength, for example, E = −0.1 V/Å, the energy of phase II is still lower than that of phase I, but the energy difference is significantly reduced (Figure 3b). A negative electric field tends to push the energy of phase II upward relative to that of phase I. Under the critical electric field E = −0.3 V/Å, the energy barrier separating these two phases disappears (Figure 3a), giving rise to a spontaneous transition from phase II to phase I (Figure 2). In contrast, a

DOI: 10.1021/jacs.5b13274
J. Am. Chem. Soc. 2016, 138, 4772−4778

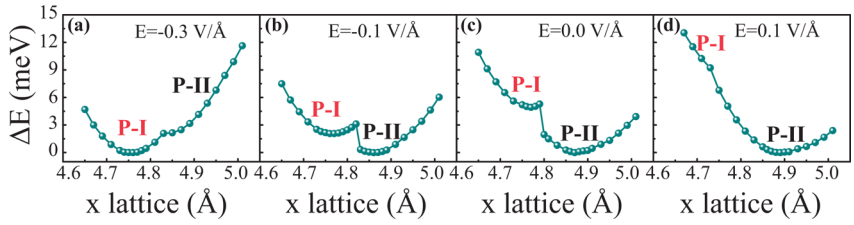

Figure 3. Relative total energy (ΔE) of P_4Li_2 versus lattice constant along x direction under an electric field of (a) −0.3, (b) −0.1, (c) 0.0, and (d) 0.1 V/Å, showing a characteristic double well profile. P-I and P-II represent phase I and phase II of P_4Li_2, respectively. Clearly the relative phase stability varies with strength of the electric field.

positive electric field pushes the relative energy of phase I upward with respect to that of phase II. Under the critical electric field E = 0.1 V/Å (Figure 3d), the energy barrier disappears and thus phase I spontaneously transforms to phase II (Figure 2).

The Bader analysis (Table S3) shows that each Li adatom donates about 0.75 electrons to the phosphorene. Applying a negative electric field (along the +z direction) would push the Li cations away from the phosphorene plane, weakening the Li−P interaction. At the critical electric field value (E = −0.3 V/Å), the stronger bonding state in phase II transforms into the weaker bonding state in phase I, as a result of increased interatomic distances. In contrast, a positive electric field (along the −z direction) will push the Li cations closer to the phosphorene plane, promoting the interaction between the Li adatom and phosphorene. Thus, it is reasonable to observe the reverse phase transition at a critical electric field strength, i.e., E = 0.1 V/Å. Some brief analysis from the energetic perspective supports this understanding (Supporting Information). These adsorbed Li atoms appear to form adatom switches. Tuning on or off these switches gives rise to the reversible structural phase transition. This adatom switch mechanism is analogous to the state-of-the-art design concept for shape memory polymers (SMPs), i.e., molecular switch.[45] But note that our adatom switch is an intramolecular interaction, in contrast to the intermolecular switches connecting different polymer molecules in SMPs.

Shape Memory Effect in P_4Li_2. The reversible phase transition in P_4Li_2 naturally gives rise to the highly desirable SME. The hysteresis loop in Figure 2 demonstrates a shape memory cycle. By taking the more stable phase II as a permanent shape, applying a negative electric field $E \leq -0.3$ V/Å will induce a phase transition to phase I. With a subsequent release of the electric field, the P_4Li_2 will remain at phase I state (as the temporary shape), finishing the shape fixing step. Subsequently, this temporary shape can recover back to the permanent shape through applying a positive electric field $E \geq 0.1$ V/Å, serving as the shape recovery step in the shape memory cycle. One unique feature of this SME in P_4Li_2 is that an electric field serves as the sole stimuli for the shape fixing and shape recovery steps, which is particularly feasible in designing nanoscale devices. This is superior to most of the conventional shape memory materials (SMMs) including shape memory alloys (SMAs) and SMPs, which are often operated via both mechanical forces and thermal temperature. Another advantage of using electric field stimuli is the high response rate, a well recognized bottleneck in conventional SMAs and SMPs owing to intrinsic difficulties of the thermal stimuli.

For conventional SMMs, the programmability is recognized as the most important attribute.[45−47] In other words, a piece of SMM should have the capability to be programmed into different temporary shapes. Such an intrinsic feature is largely enabled by the coexistence of different phases/variants in microstructures of SMMs, e.g., different domain patterns caused by movement of domain walls in SMAs.[32] As the result, various combinations of distinct phases/variants in one SMM will yield multiple temporary shapes. We thus examined the coexistence of both phases. Figure S5 summarizes different combinations of phase I and phase II in a supercell including total N = 6 units and N' units of phase I. Different cases are examined, where N'/N varies from 2/6 up to 4/6. Our DFT simulations allowed determination of the stability of all these supercells, indicating the stable coherent existence of two phases in a single crystal and thereby the programmability.

We propose a prototypic design to demonstrate the programmability of P_4Li_2, as presented in Figure 4a. Applying a local electric field via an STM or AFM tip will cause local phase transition, forming phase I domains in the phase II matrix. After release of the local electric field, a temporary shape

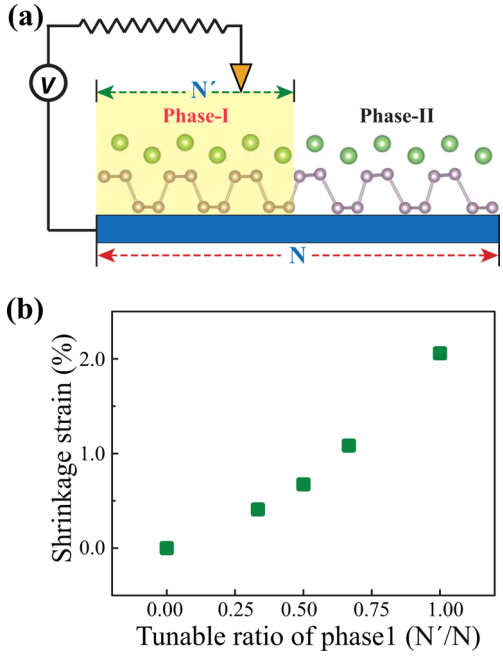

Figure 4. (a) A simple design to realize different temporary shapes in one piece of P_4Li_2, that is, programmability. In light of the stable coexistence of phase I and phase II in one supercell (Figure S3), using an AFM or STM tip to apply a local electric field to different regions (causing local phase transition) should yield different stable temporary shapes. (b) The tunable strains arising from the possible temporary shapes in a supercell with 6 unit cells (N = 6), where N' is the number of unit cells under the local electric field.

DOI: 10.1021/jacs.5b13274
J. Am. Chem. Soc. 2016, 138, 4772−4778

will be fixed. By changing the location and size of phase I domains via control of the local electric fields, different temporary shapes can be defined. This programing procedure is analogous to forming temporary shapes by mechanical loading caused deformation in SMA or SMP. Taking the 6-unit supercell as an example, changing the region (N' unit-cells) of the applied local electric field can generate multiple temporary shapes (Figure S5). Figure 4b summarizes the strain outputs arising from these temporary shapes. The maximum recoverable strain is 2.06%, much higher than most strain outputs stemming from the piezoelectricity, electroactive effect, and quantum effect in other 2D materials. In the shape recovery step, a global uniform electric field in an opposite direction will transform the whole material back to the permanent phase II structure.

Besides the normal one-way SME, the two-way shape memory effect (TWSME) has attracted intensive research interests in the past few years.[48] The TWSME refers to a phenomenon that once a desired temporary shape fixing is accomplished, applying and releasing certain external stimuli can trigger the shape change between the permanent and temporary shape repeatedly. It appears that the material can memorize both shapes. This TWSME is highly desirable for shape memory devices that are able to change its shape reversibly many times without the necessity to employ an extra reprogramming procedure (often using different types of stimuli) by the users. TWSME offers unique features in device designs; however, there are very few SMMs with TWSME.[48]

We propose that our P_4Li_2 might have a pseudo-TWSME. Note that the reversible phase transition is triggered by the electric field only. In practice, after a local electric field is applied to fix a determined temporary shape, the same type of local electric field but along an opposite direction could be employed to recover its original shape, effectively acting as a release of stimuli in TWSME. This procedure is infinitely repeatable in theory. It seems that both original and temporary shapes are memorized and can be recovered with electric fields in opposite directions. We believe it shares the same characteristics of TWSME and thus would call it pseudo-TWSME. The design principles and routes of utilizing TWSME in various devices should be applicable to our P_4Li_2.

It is worth noting that the small energy difference between phase I and phase II (~10 meV) suggests that a mixture of the two phases can happen at a high temperature (>100 K). We expect that the electric field induced reversible phase transition might also be observable for such a mixed phase case. From Figure 2, applying a negative (global or local) $E < -0.3$ V/Å would always cause phase II (completely or partly) in the phase mixture to transit to phase I, because phase II is a not stable phase under this E-field (Figure 3). It is the same for the phase transition from phase I to phase II under a positive E-field. After releasing the E-field, the new phase (or phase mixtures) would (at least) temporarily maintain their states. It is reasonable to expect that, after a period of time (depending on temperature), thermal excitation will lead to a phase mixture again and hence the effect of the E-field induced phase transition would diminish. But for electromechanical actuation applications at a high operation frequency (e.g., MHz to GHz), the SME of P_4Li_2 might still be applicable at a relatively high temperature (>100 K). We, therefore, believe that the E-field induced reversible phase transition and the resultant SME should apply under a low temperature (<~100 K) and might also be useful for high actuation frequency applications under a relatively high temperature.

Recently the reversible structural phase transition has been reported for some 2D materials at room temperature.[40,41] Using DFT simulations, Duerloo et al. reported an interesting structural phase transition for transition metal dichalcogenide (TMD) systems via a combination of mechanical loading and thermal excitation.[40] For $MoTe_2$, they found that, with application of uniaxial tensile force or biaxial (hydrostatic in 2D) tensile stress, 2H to 1T′ phase transition should take place with the help of thermal excitation at room temperature. In the opposite direction, under a uniaxial compressive force or biaxial compressive stress, the 1T′ phase could, in principle, transit to the 2H phase. But in practice, the compressive stress could easily cause buckling of the thin TMD materials and thus the reverse phase transition may not happen. Ma et al. reported the reversible semiconducting-to-metallic phase transition (2H to 1T) in MoS_2 via *n*-BuLi chemical treatment and thermal annealing.[41] But it is a very slow process, taking more than 48 h for the transition to happen. Our reported reversible phase transition and the SME have several clear advantages. First, in NEMS applications, applying the E-field is much more feasible and easy to control than applying temperature or force stimuli. The electromechanical energy conversion is the most popular option in NEMS. Second, since there is no (slow) thermal excitation involved, our P_4Li_2 is very promising for high frequency applications, up to the MHz to GHz range. Note that a well-recognized bottleneck of available SMMs is the low actuation frequency (~1 Hz).

Superelasticity. Superelasticity (SE) is another special phenomenon for SMMs. Its key characteristic is a plastic-like strain plateau in nonlinear superelastic stress−strain relation as a result of stress induced phase transitions.[32] Superelasticity has a broad range of applications as sensors, actuators, and energy storage devices.[49−52]

We also observed the superelasticity in the P_4Li_2 crystal under specific electric fields. Figure 5 shows a stress−strain relation with a characteristic plastic-like strain plateau for P_4Li_2 under an electric field $E = -0.3$ V/Å. Owing to the 2D nature, the edge stress is expressed as force per unit edge length.[53] Phase I is the single stable phase under this electric field strength (Figure 3a). Stretching it yields a linear stress−strain

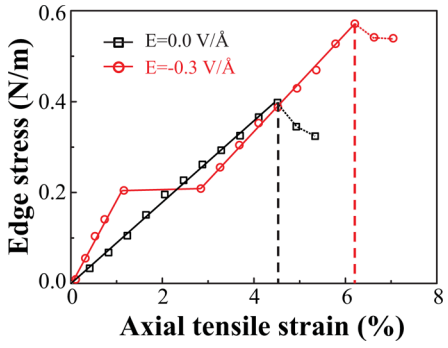

Figure 5. Nonlinear superelastic stress−strain relation for P_4Li_2 crystal in armchair (x) direction under an electric field of −0.3 V/Å. The characteristic plastic-like strain plateau can be seen, where a stress induced phase transition takes place. The stress−strain relation of P_4Li_2 under zero electric field is also shown for a comparison. Note that in the former case the equilibrium structure of P_4Li_2 is phase I, whereas for the latter case it is phase II (Figure 3).

DOI: 10.1021/jacs.5b13274
J. Am. Chem. Soc. 2016, 138, 4772−4778

relation up to 1.5% tensile strain (corresponding to the transition point connecting phase I and phase II in the energy curve), above which a stress induced phase transition takes place (Figure S4). Provided a constant stress condition, the P_4Li_2 structure will jump to phase II, leading to a sudden increase of strain value to 2.8% (Supporting Information). The resultant plateau should be interpreted as growth of phase II domains while increasing strain. Releasing the force will result in P_4Li_2 spontaneously returning to its original phase I shape due to the absence of an energy barrier. Figure S7 shows a similar superelastic behavior for P_4Li_2 under electric field E = 0.1 V/Å while being subjected to a compressive force. The plateau starts at a compressive strain of 2.9% and ends at 4.9%.

An obvious benefit of SE is a significant enhancement of mechanical yield point. Figure 5 shows that the maximum tensile elastic strain of the P_4Li_2 phase II is 4.5% (under a zero electric field), whereas it is enhanced to 6.2% under an electric field E = −0.3 V/Å. Similarly, its ideal compressive elastic strain will be enhanced to 6.6% (under electric field E = 0.1 V/Å) from 5.0% (under a zero electric field). From Figure 5, the two-dimensional elastic modulus along the armchair direction (x-direction) can be determined. Phase I has a modulus of 13.34 N/m (0.83 eV/Å^2), which is almost the same as that of pure phosphorene (13.33 N/m).[54] Phase II has a much smaller modulus at 8.78 N/m (0.55 eV/Å^2). This could be attributed to the distorted upper layer of P atoms in phase II.

The above discussions are under ideal conditions, and the effects of phase boundaries (Figure 4) are not included. Considering the nucleation and growth of new phases during phase transitions, a hysteresis loop should appear in the stress−strain curve, as usually observed for superelastic materials.[32] This stress−strain hysteresis loop could be useful for energy damping applications at the nanoscale.[52]

CONCLUSIONS

In summary, using *ab initio* DFT simulations, we find two stable phases in Li adsorbed phosphorene (P_4Li_2), which show distinctive structures and electronic properties. Phase II is stabilized by the enhanced Li and P atom interaction evidenced by the clear charge transfer and the Li *s*- and P *p*-orbital hybridizations, named as adatom switches. Our DFT simulations demonstrate that an external electric field can turn on or off the adatom switches and thus trigger reversible phase transition between phase I and phase II, naturally giving rise to the highly desirable shape memory effect and superelasticity in the 2D materials. These phenomena have not been reported for 2D materials before. Our results also demonstrate the stable coexistence of these two phases, implying programmability of the P_4Li_2 crystal. The tunable recoverable strain is up to 2.6%, significantly higher than most electromechanical strain outputs in other 2D materials. Superelasticity is also observed in P_4Li_2, which significantly enhances the tensile strain limit from 4.5% to 6.2%. Together with an atomic thickness, superior flexibility, the excellent electromechanical strain outputs, and the special properties arising from SME or SE (such as desirable shape fixing and energy damping) endow P_4Li_2 with great application potential for energy conversion at the nanoscale and in novel NEMS devices.

ASSOCIATED CONTENT

Supporting Information

The Supporting Information is available free of charge on the ACS Publications website at DOI: 10.1021/jacs.5b13274.

DFT simulation details (PDF)

AUTHOR INFORMATION

Corresponding Authors

*zhe.liu@monash.edu

*junkai.deng@mail.xjtu.edu.cn

Notes

The authors declare no competing financial interest.

ACKNOWLEDGMENTS

We gratefully acknowledge support from the National Science Foundation of China (Grants Nos. 51471126, 2012CB619401, 51320105014, 51321003, 51431007, and IRT13034) and the Australian Research Council. The simulation work was carried out using high performance computing facilities from National Computational Infrastructure through the NCMAS scheme.

REFERENCES

(1) Novoselov, K. S.; Geim, A. K.; Morozov, S. V.; Jiang, D.; Zhang, Y.; Dubonos, S. V.; Grigorieva, I. V.; Firsov, A. A. *Science* **2004**, *306*, 666.

(2) Neto, A. H. C.; Novoselov, K. *Mater. Express* **2011**, *1*, 10.

(3) Xu, M.; Liang, T.; Shi, M.; Chen, H. *Chem. Rev.* **2013**, *113*, 3766.

(4) Butler, S. Z.; et al. *ACS Nano* **2013**, *7*, 2898.

(5) Jariwala, D.; Sangwan, V. K.; Lauhon, L. J.; Marks, T. J.; Hersam, M. C. *ACS Nano* **2014**, *8*, 1102.

(6) Wang, Q. H.; Kalantar-Zadeh, K.; Kis, A.; Coleman, J. N.; Strano, M. S. *Nat. Nanotechnol.* **2012**, *7*, 699.

(7) Zhang, Y.; Tang, T. T.; Girit, C.; Hao, Z.; Martin, M. C.; Zettl, A.; Crommie, M. F.; Shen, Y. R.; Wang, F. *Nature* **2009**, *459*, 820.

(8) Oostinga, J. B.; Heersche, H. B.; Liu, X.; Morpurgo, A. F.; Vandersypen, L. M. *Nat. Mater.* **2008**, *7*, 151.

(9) Wang, Y.; Ou, J. Z.; Balendhran, S.; Chrimes, A. F.; Mortazavi, M.; Yao, D. D.; Field, M. R.; Latham, K.; Bansal, V.; Friend, J. R.; Zhuiykov, S.; Medhekar, N. V.; Strano, M. S.; Kalantar-zadeh, K. *ACS Nano* **2013**, *7*, 10083.

(10) Bunch, J. S.; Verbridge, S. S.; Alden, J. S.; van der Zande, A. M.; Parpia, J. M.; Craighead, H. G.; McEuen, P. L. *Nano Lett.* **2008**, *8*, 2458.

(11) Deng, J.; Liu, J. Z.; Medhekar, N. V. *RSC Adv.* **2013**, *3*, 20338.

(12) Zhao, Y.; Song, L.; Zhang, Z.; Qu, L. *Energy Environ. Sci.* **2013**, *6*, 3520.

(13) Wang, Z.; Feng, P. X. L. *Appl. Phys. Lett.* **2014**, *104*, 103109.

(14) Wu, W.; Wang, L.; Li, Y.; Zhang, F.; Lin, L.; Niu, S.; Chenet, D.; Zhang, X.; Hao, Y.; Heinz, T. F.; Hone, J.; Wang, Z. L. *Nature* **2014**, *514*, 470.

(15) Wang, X.; Shi, G. *Energy Environ. Sci.* **2015**, *8*, 790.

(16) Rogers, G. W.; Liu, J. Z. *J. Am. Chem. Soc.* **2012**, *134*, 1250.

(17) Rogers, G. W.; Liu, J. Z. *Appl. Phys. Lett.* **2013**, *102*, 021903.

(18) Rogers, G. W.; Liu, J. Z. *J. Am. Chem. Soc.* **2011**, *133*, 10858.

(19) Ong, M. T.; Reed, E. J. *ACS Nano* **2012**, *6*, 1387.

(20) Duerloo, K. A. N.; Ong, M. T.; Reed, E. J. *J. Phys. Chem. Lett.* **2012**, *3*, 2871.

(21) Xie, X.; Bai, H.; Shi, G.; Qu, L. *J. Mater. Chem.* **2011**, *21*, 2057.

(22) Liang, J.; Huang, Y.; Oh, J.; Kozlov, M.; Sui, D.; Fang, S.; Baughman, R. H.; Ma, Y.; Chen, Y. *Adv. Funct. Mater.* **2011**, *21*, 3778.

(23) Chandrakumara, G. G.; Shang, J.; Qiu, L.; Fang, X.-Y.; Antolasic, F.; Easton, C. D.; Song, J.; Alan, T.; Li, D.; Liu, J. Z. *RSC Adv.* **2015**, *5*, 68052.

(24) Sun, G.; Kertesz, M.; Kürti, J.; Baughman, R. H. *Phys. Rev. B: Condens. Matter Mater. Phys.* **2003**, *68*, 125411.

DOI: 10.1021/jacs.5b13274
J. Am. Chem. Soc. 2016, 138, 4772−4778

(25) Bechmann, R. *Phys. Rev.* **1958**, *110*, 1060.
(26) Lueng, C. M.; Chan, H. L.; Surya, C.; Choy, C. l. *J. Appl. Phys.* **2000**, *88*, 5360.
(27) Liu, H.; Neal, A. T.; Zhu, Z.; Luo, Z.; Xu, X.; Tománek, D.; Ye, P. D. *ACS Nano* **2014**, *8*, 4033.
(28) Li, L.; Yu, Y.; Ye, G. J.; Ge, Q.; Ou, X.; Wu, H.; Feng, D.; Chen, X. H.; Zhang, Y. *Nat. Nanotechnol.* **2014**, *9*, 372.
(29) Li, W.; Yang, Y.; Zhang, G.; Zhang, Y. W. *Nano Lett.* **2015**, *15*, 1691.
(30) Guan, J.; Zhu, Z.; Tománek, D. *Phys. Rev. Lett.* **2014**, *113*, 046804.
(31) Guan, J.; Zhu, Z.; Tománek, D. *ACS Nano* **2014**, *8*, 12763.
(32) Otsuka, K.; Wayman, C. M. *Shape memory materials*; Cambridge University Press: 1999.
(33) Kresse, G.; Furthmüller, J. *Phys. Rev. B: Condens. Matter Mater. Phys.* **1996**, *54*, 11169.
(34) Kresse, G.; Joubert, D. *Phys. Rev. B: Condens. Matter Mater. Phys.* **1999**, *59*, 1758.
(35) Heyd, J.; Scuseria, G. E.; Ernzerhof, M. *J. Chem. Phys.* **2003**, *118*, 8207.
(36) Carter, E. A. *Science* **2008**, *321*, 800.
(37) Hu, T.; Hong, J. *J. Phys. Chem. C* **2015**, *119*, 8199.
(38) Our HSE06 calculations also confirm the stability of both phases and a similar total energy difference. The lattice constants of both phases calculated using the HSE06 method are quite close to PBE results. See Table S1 in the Supporting Information.
(39) Mehboudi, M.; Dorio, A. M.; Zhu, W.; van der Zande, A.; Churchill, H. O. H.; Pacheco-Sanjuan, A. A.; Harriss, E. O.; Kumar, P.; Barraza-Lopez, S. *arXiv preprint arXiv:1510.09153* 2015.
(40) Duerloo, K.-A. N.; Li, Y.; Reed, E. J. *Nat. Commun.* **2014**, *5*, 4212.
(41) Ma, Y.; Liu, B.; Zhang, A.; Chen, L.; Fathi, M.; Shen, C.; Abbas, A. N.; Ge, M.; Mecklenburg, M.; Zhou, C. *ACS Nano* **2015**, *9*, 7383−7391.
(42) Chang, Z.; Yan, W.; Shang, J.; Liu, J. Z. *Appl. Phys. Lett.* **2014**, *105*, 023103.
(43) Shimada, K. *Jpn. J. Appl. Phys.* **2006**, *45*, L358.
(44) Hangleiter, A.; Hitzel, F.; Lahmann, S.; Rossow, U. *Appl. Phys. Lett.* **2003**, *83*, 1169.
(45) Zhao, Q.; Qi, H. J.; Xie, T. *Prog. Polym. Sci.* **2015**, *49-50*, 79.
(46) Jani, J. M.; Leary, M.; Subic, A.; Gibson, M. A. *Mater. Eng.* **2014**, *56*, 1078.
(47) Leng, J.; Lan, X.; Liu, Y.; Du, S. *Prog. Mater. Sci.* **2011**, *56*, 1077.
(48) Hager, M. D.; Bode, S.; Weber, C.; Schubert, U. S. *Prog. Polym. Sci.* **2015**, *49-50*, 3.
(49) Otsuka, K.; Ren, X. *Prog. Mater. Sci.* **2005**, *50*, 511.
(50) Otsuka, K.; Kakeshita, T. *MRS Bull.* **2002**, *27*, 91.
(51) Li, S.; Ding, X.; Li, J.; Ren, X.; Sun, J.; Ma, E. *Nano Lett.* **2010**, *10*, 1774.
(52) Juan, J. S.; No, M. L.; Schuh, C. A. *Nat. Nanotechnol.* **2009**, *4*, 415.
(53) Deng, J.; Fampiou, I.; Liu, J. Z.; Ramasubramaniam, A.; Medhekar, N. *Appl. Phys. Lett.* **2012**, *100*, 251906.
(54) Peng, X.; Wei, Q.; Copple, A. *Phys. Rev. B: Condens. Matter Mater. Phys.* **2014**, *90*, 085402.

DOI: 10.1021/jacs.5b13274
J. Am. Chem. Soc. 2016, 138, 4772−4778